MINISTRY OF EDUCATION
AND TRAINING

VIETNAM ACADEMY OF
SCIENCE AND TECHNOLOGY

GRADUATE UNIVERSITY OF SCIENCE AND TECHNOLOGY

Chu Anh Tuan

SYNTHESIS AND OPTICAL PROPERTIES OF Ce AND Eu-DOPED ZnS QUANTUM DOTS AND QUANTUM DOTS BASED ON CdSe, CdS DISPERSED IN WATER AND COATED WITH SILICA

SUMMARY OF DISSERTATION ON SOLID STATE PHYSICS
Code: 9440104

Hanoi, 2025

The dissertation is completed at: Graduate University of Science and Technology, Vietnam Academy of Science and Technology

Supervisors:

1. Supervisor 1: **Assoc.Prof, Dr. Chu Viet Ha**, Thai Nguyen University of Education
2. Supervisor 2: **Assoc.Prof, Dr. Tran Hong Nhung**, Institute of Physics, Vietnam Academy of Science and Technology

Referee 1:...

Referee 2:...

Referee 3:...

The dissertation will be examined by Examination Board of Graduate University of Science and Technology, Vietnam Academy of Science and Technology at……………………….. (time, date……)

The dissertation can be found at:

1. Graduate University of Science and Technology Library
2. National Library of Vietnam

INTRODUCTION

Advances in nanotechnology and research have led to new fluorescent labelling systems with superior luminance and optical stability compared to traditional organic fluorescent materials. These are luminescent nanoparticles created on semiconductor nanomaterials, commonly known as quantum dot nanoparticles. The emergence of this class of fluorescent labelling or labelling materials plays a vital role in studying processes occurring in biological objects such as cells and molecules.

Quantum dots made from semiconductor compounds of the $A^{II}B^{VI}$ group, one of the most exciting objects in nanomaterials with a straight band gap structure, are suitable for existing optical excitation sources. Quantum dots in this group include materials such as CdS (cadmium sulfide), CdSe (cadmium selenide) and CdTe (Cadmium telluride) - with bulk semiconductor band gaps of 2.49 eV, 1.8 eV and 1.5 eV respectively; so when at nanometer size, these semiconductors can emit fluorescence at any wavelength in the visible region. In addition to CdSe quantum dots with a huge amount of research on properties, fabrication methods and application capabilities, CdS quantum dots are also one of the typical $A^{II}B^{VI}$ semiconductor materials, which have been studied in Vietnam since the 2000s and have many remarkable achievements. Compared to CdSe quantum dots, the fabrication of CdS quantum dots makes it more challenging to create quantum dots with uniform size distribution and less affected by surface states. CdS quantum dots, along with other Cadmium-based $A^{II}B^{VI}$ quantum dots, have unique optical properties that are different from bulk semiconductors, such as controllable effective band gap, strong charge separation effect, significant Stokes shift and good optical stability. These properties indicate their significant potential for applications in fluorescence detectors, sensors, solar cells, light-emitting diodes (LEDs) and other fields.

Rare-earth doped optical materials have achieved remarkable achievements in research as well as in applications. However, doped quantum dot materials are still attractive because studies on doped quantum dots have only been carried out on some quantum dot systems, such as ZnO or carbon. These quantum dots have been studied and are promising as potential materials for applications in cell sensing and monitoring, photocatalysis, solar cells, and optoelectronic devices. Thus, extending the doping to other quantum dot systems will produce material systems with many new properties, promising much potential in different applications.

In the $A^{II}B^{VI}$ semiconductor family, ZnS (Zinc Sulfide) semiconductors are the focus of much research because this is a semiconductor that also has a straight band gap, a large band gap ($E_g \sim 3.68$eV at room temperature), and high-temperature stability... so it can be used as a shell for core/shell structured quantum dots with the core being semiconductors with a smaller band gap; or as a host for doped quantum dots. Therefore, ZnS quantum dots and the $A^{II}B^{VI}$ group with core/shell and doped structures will open up many valuable applications. In addition to their outstanding ability as markers, when doped, quantum dots will create a material system with fluorescence emission at longer wavelengths, such as red and far red, which can be applied in solid-state lighting devices and increase the ability to self-produce fluorescent materials in our country. With the appropriate technique, many quantum dots can be incorporated into a silica nanoparticle, giving it enhanced luminosity and amplified optical signals compared to single quantum dots, promising improved sensitivity in optical analysis. Moreover, the SiO_2 layer will also increase the durability of the quantum dot material under the stimulation of ultraviolet radiation. When coated with a silica shell, quantum dots will also have higher mechanical, electrical and chemical durability.

Based on the above facts, the dissertation has been carried out to focus on two main research directions: Research on ZnS quantum dots doped with rare earth ions for light-emitting applications and research on quantum dots based on CdSe, CdS semiconductors dispersed in water and coated with oriented silica for biomedical fluorescent labelling applications.

The selected dissertation's title is: "*Synthesis and optical properties of Ce and Eu-doped ZnS quantum dots and quantum dots based on CdSe, CdS dispersed in water, and coated with silica*".

Objectives

The objectives of the dissertation focus on:

- Fabrication and investigation of optical properties of ZnS quantum dots doped with some rare earth ions for emission applications
- Fabrication and investigation of optical properties of quantum dots such as CdSe, CdSe/CdS, CdS, CdS/ZnS dispersed in water to minimize toxic chemicals suitable for use as fluorescent markers.
- Fabrication and investigation of properties of silica nanoparticles containing quantum dots for biological labeling applications.

Research scope and content

i/ Research on the fabrication and investigation of the optical properties of ZnS quantum dots doped with Ce and Eu rare earth ions for emission applications.

ii/ Research on the fabrication and optical properties of quantum dots synthesized from semiconductor compounds of the $A^{II}B^{VI}$ group (CdSe, CdSe/CdS, CdS, CdS/ZnS) dispersed in water via a green method using suitable safe chemicals as fluorescent markers.

iii/ Research on the fabrication and characteristics of silica nanoparticles containing quantum dots by the Stöber method for biomedical labeling applications

The scientific significance of the thesis

The dissertation “Synthesis and optical properties of (Ce, Eu)-doped ZnS quantum dots and quantum dots based on CdSe, CdS dispersed in water and coated with silica” has been studied firstly in Vietnam about the fabrication of ZnS quantum dots co-doped with rare earth elements Ce and Eu for white light emission applications; and investigation of the energy transfer mechanism of these rare earth ions in the ZnS quantum dot host. The thesis has also focused on fabricating $A^{II}B^{VI}$ quantum dots directly in an aqueous environment using citrate as a surfactant to control the size - reducing toxicity and danger compared to the synthesis of quantum dots in organic solvents at high temperatures. It has also systematically studied the synthesis of silica nanoparticles containing quantum dots dispersed in water by the Stöber method under initial conditions oriented for labelling applications.

Chapter 1

OVERVIEW OF RESEARCH ISSUES

1.1. Properties and some issues related to quantum dots

1.1.1. Some features of quantum dots and quantum confinement effect

In quantum dots, the charge carriers are electrons, holes, or excitons confined in all three dimensions. The system is described as an infinite three-dimensional potential well: the potential is zero everywhere in the potential well and infinite at the walls of the well. The quantum confinement of the charge carriers disrupts their energy levels along the confined direction and thus changes the density of states according to the energy of the charge carriers.

Currently, the theory of quantum dots has been entirely built. The physical processes occurring in a quantum dot and manifesting their external properties have been deeply understood and recognized. The size of a semiconductor quantum dot can be determined entirely by its optical absorption spectrum or its fluorescence excitation spectrum. The optical properties of quantum dots are completely explained in terms of mechanism through quantum mechanics.

1.1.2. Energy levels of carriers in quantum dots

The energy levels of quasi-particles in quantum dots are changed compared to bulk semiconductor materials due to the quantum confinement effect that occurs for these particles when the material size is small and comparable to their de Broglie wavelength, or comparable to the Bohr radius of excitons in semiconductors. Based on the variational approximation method, it is found that the energy in the ground state (1s1s) of the electron-hole pair can be expressed as (Kayanuma formula)

$$E_{1s1s} = E_g + \frac{\hbar^2\pi^2}{2\mu a^2} - 1.786\frac{e^2}{\varepsilon a} - 0.248R_y^*$$

where E_g is the band gap energy of bulk semiconđuctor, μ is the reduced mass of electrons and holes, a is radius of the quan tum dots, R^*_y is Rydberg energy. The formular is used to estimate the size of quantum dots.

1.1.3. Optical properties of quantum dots

Their highly tunable optical properties are desirable based on their size, leading to many research and commercial applications, including bioimaging, solar cells, LEDs, diode lasers, and transistors.

Theoretical and experimental studies have shown that the luminescence lifetimes corresponding to exciton transitions in quantum dots range from tens to hundreds of nanoseconds, much larger than the luminescence lifetimes of excitons in bulk materials, which typically range from several hundred picoseconds to sub-nanoseconds. Quantum Yield or Fluorescence Quantum Yield is one of the essential characteristics of fluorescent materials and is of particular interest for luminescent nanoparticles in general and quantum dots in particular. For quantum dots that are purely semiconductors (i.e., only cores), the quantum efficiency is usually low, not as high as that of dyes. For core/shell nanostructured quantum dots, the quantum efficiency can reach 70–80% due to the limitation of surface states and dangling bonds of the core semiconductor.

Quantum dot blinking is a phenomenon in which photogenerated carriers continue to escape from the quantum dot for a period of time that can last up to several seconds before returning and causing luminescence forming off states and occurring at the single-particle level. Blinking can be suppressed when the quantum dots are encapsulated with another inert shell..

1.1.4. The toxicity of quantum dots

Quantum dots based on semiconductors such as CdSe, CdS, and CdTe are often harmful to cells and biological objects. Many studies have shown that they are highly toxic. Quantum dots coated with molecules such as mercaptoacetic acid, mercaptopropionic acid, 11-mercaptoundecanoic acid, and 2-aminoethanethiol can generate toxic ions such as Cd+2 and S-2. Methods to reduce the toxicity of quantum dots include coating quantum dots in elements such as bovine serum albumin (BSA) or polyethylene glycol (PEG) or coating them in an inert shell such as a silica shell.

1.2. Rare earth-doped luminescent materials and quantum dots

There have been many studies on quantum dots doped with transition metal ions or rare earth ions. These added impurities provide additional carriers for the quantum dots and impurity centres that can interact with the electron-hole pairs of the quantum dots. Then, an energy transfer mechanism will occur from the quantum dots to the impurity centres. Thus, these impurity centres do not affect the absorption spectrum, but due to the energy transfer mechanism, they enormously change the fluorescence emission properties of the quantum dots. Moreover, when doped into quantum dots, the emission efficiency of these luminescent centres will increase, and the emission time will be shortened due to the quantum confinement effect. Therefore, quantum dots doped with rare earth ions are attracting much research attention, promising many potential applications in the lighting field.

1.2.1. Eu ion in solid substrates

Europium (Eu) ion is one of the rare earth ions in the lanthanoid family. It is also one of the widely studied ions because their fluorescence emission is suitable for photonics and optical communication applications. When the Eu^{3+} ion is excited and jumps to a higher energy level in a solid substrate, it will quickly recover to a lower energy level and emit radiation with wavelengths in the visible region. These radiations correspond to the transitions from the excited level 5D0 to the levels ^7F_j (j= 0, 1, 2, 3, 4, 5, 6) of the $4f^6$ configuration. The $^5D_0$ energy level is not split by the crystal field (J=0); the splitting of the emission transitions is caused by the splitting of the crystal field on the ^7F_j energy levels. The Eu^{3+} ion has a powerful emission in the visible light region. After being excited with a minimum energy of 2.18 eV, the electrons will move to the $^5D_0$ excited energy level, recover to the ground energy level $^7F_2$, and emit red light with a wavelength of 614 nm. It is the typical emission wavelength of Eu^{3+} ions in a solid crystal lattice.

1.2.2. Rare earth element Ce and Ce-doped nanomaterials

The Ce element is located at position 58 in the Mendeleev periodic table, with the electron configuration [Xe] $4f^1 5s^2 5p^6 5d^1 6s^2$. When the Ce atom loses 3 electrons at $5d^1 6s^2$, it becomes a Ce^{3+} ion, and its electron configuration is now [Xe] $4f^1 5s^2 5p^6$. The Ce^{3+} ion has a strong emission band and a broad absorption band due to the allowed transitions between the $4f^7$ and $4f^6 5d^1$ energy states; these transitions are highly dependent on the nature of the substrate material – highly dependent on the type of crystal field. Therefore, the emission of the Ce^{3+} ion can be controlled in a wide wavelength range from violet to visible. It can lead to the versatility of Ce^{3+} ions for applications as optical excitation centres.

Under the conditions of the thesis, I chose ZnS nanomaterials doped with Eu and Ce ions for studies on luminescent nanomaterials applied in lighting devices because doping can control the emission wavelength of the ZnS nanomaterial system in the visible region. The optical properties of this material system will be studied by absorption, fluorescence, and photoluminescence lifetime measurements.

1.3. Research on synthesis of semiconductor nanoparticles and quantum dots

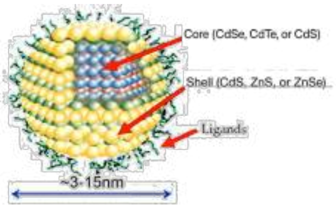

Figure 1. *Illustration of the structure of a quantum dot that can be dispersed in biological media*

Figure 1 shows a common model of the structure of quantum dots used for biolabeling. The core material of the quantum dot is a semiconductor material capable of emitting fluorescence with high photostability, which is used to perform fluorescent labelling. The shell material of the quantum dot is usually a semiconductor with a larger band gap than the core material so as not to affect the core's fluorescence emission process and increase the core's emission efficiency by limiting dangling bonds and surface states. The surface of the quantum dot is covered with ligand molecules with functional groups, helping the quantum dot disperse nicely in the solution. These ligand molecules are usually hydrophilic molecules. The size of these quantum dots is usually less than 10 nm.

This thesis will conduct research on the fabrication of water-soluble quantum dot systems, including CdSe/CdS and CdS/ZnS. These quantum dots will be manufactured directly in an aqueous environment using a citrate compound to control quantum dot size, synthesized under low-temperature conditions (below the boiling temperature of water) according to the cleanest and safest criteria possible.

1.4. Research on synthesis of silica nanoparticles containg quantum dots

Fluorescent silica nanoparticles are silica nanoparticles that contain fluorescent emitting centres, which can be organic dyes, quantum dots, or rare earth ions. The Stöber method has also been proposed to synthesize quantum dot-containing silica nanoparticles, which have remarkable fluorescence efficiency and are suitable for biolabeling applications. Figure 2 illustrates several models for the fabrication of quantum dot-containing silica nanoparticles: quantum dots dispersed in a silica shell (figure a), dispersed in silica nanoparticles (figure b), or simply single quantum dots encapsulated in a thin silica shell (figure c).

The fabrication of quantum dot-containing silica nanoparticles by forming a SiO_2 shell around the quantum dots is beneficial in biomedical applications such as labelling and imaging. However, in biological applications, quantum dots are usually types of colloidal, such as CdTe/ZnS, CdSe/ZnS, and CdSe/CdS, which have a negative charge on their surface. Research has shown that the silica network formed through hydrolysis and condensation processes also carries a negative charge, therefore, it is challenging to introduce quantum dots into the silica matrix because they can be pushed out due to the same electric charge as the silica matrix.

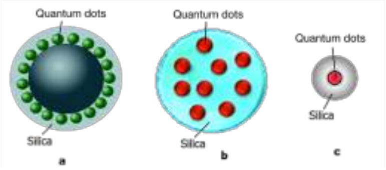

Figure 2. *Illustration of some models of silica nanoparticle containing quantum dots*

Chapter 2

SYNTHESIS AND OPTICAL PROPERTIES OF Ce, Eu DOPED AND CO-DOPED ZnS QUANTUM DOTS FOR EMISSION APPLICATIONS

Semiconductor ZnS quantum dots (QDs) co-doped with Eu^{3+} and Ce^{3+} were synthesized by the chemical method. The optical properties of the samples were characterized by absorption spectroscopy, photoluminescence (PL) spectroscopy and PL-decay lifetime. X-ray diffraction revealed that the QDs had a zincblende structure and a particle size of about 3 nm. The presence of Eu^{3+} and Ce^{3+} ions in the samples were proved by X-ray photoelectron spectroscopy. For Ce^{3+} and Eu^{3+} ions co-doped in ZnS QDs, the luminescence intensity and lifetime of the $5d^1$ (Ce^{3+}) level decrease while the emission intensity of Eu^{3+} ion increases with the increasing Eu^{3+}concentration. The reduced lifetime and the luminescence quenching of the $5d^1$ (Ce^{3+}) level are due to the energy transfer from Ce^{3+} to Eu^{3+} ion. The properties of ligand field and the intensity parameters of Eu^{3+} doped ZnS QDs and the efficiency of the energy transfer process from Ce^{3+} ions to Eu^{3+} ions and the nature of this interaction mechanism were expalained by theoretical models.

2.1. Synthesis of Eu/Ce-doped and (Eu, Ce) co-doped ZnS quantum dots

One-pot synthesis was used to fabricate Eu/Ce-doped and (Eu, Ce) co-doped ZnS QDs using oleic acid (OA), tri-n-octylphosphine (TOP), and Octadecene (ODE) in toluene at high temperatures . First, a solution of S^{2-} ions was prepared by dissolving S powder (1 mmol) in TOP (1 ml) and ODE (5 ml) at 100 °C combining with constant stirring. Second, $Zn(CH_3COO)_2·2H_2O$ (1 mmol), OA (2 ml), and ODE (30 ml) were mixed in a three-neck flask and then placed for 1 h at 240 °C with continuous stirring to produce a homogeneous solution containing Zn^{2+} ions. Eu^{3+} and/or Ce^{3+} solutions were prepared by dissolving $Eu(CH_3CO_2)_3·H_2O$ and/or $Ce(CH_3CO_2)_3·H_2O$ in TOP and ODE at 150 °C until the solution became clearly homogeneous. To synthesize the doped-QDs, Zn^{2+} solution was mixed with a solution containing a specific amount of Eu^{3+}/Ce^{3+} and (Eu^{3+},Ce^{3+}), which were calculated according to the Eu^{3+},Ce^{3+}/Zn^{2+} and $(Eu^{3+}/Ce^{3+})/Zn^{2+}$ ratios. Then, the S^{2-} solution was swiftly injected into the mixture at 240 °C. For growing of Eu/Ce-doped and (Eu, Ce) co-doped ZnS QDs, the reaction system was maintained at 240 °C for 60 min. The obtained solution containing QDs was cooled down to room temperature and mixed with isopropanol. The as-synthesized QDs were separated from the liquid by centrifugation at the speed of 10,000 rpm for 5 min. The collected sediment of Eu, Ce-doped and (Eu, Ce) co-doped ZnS QDs were dispersed in toluene for study their physical properties afterward. All of the synthesis processes were performed in a nitrogen atmosphere to avoid oxidation.

Figure 3 presents the TEM images of ZnS and $ZnS{:}Ce^{3+}/Eu^{3+}$ QDs; the QDs are quite monodisperse in solution with sizes of several nm.

A spectrofluorometer (Horiba Jobin Yvon Fluoromax-4) was used to measure photoluminescence (PL), photoluminescence excitation (PLE) spectra and luminescence lifetime (using the xenon lamp as an excitation source). Ultraviolet–visible (UV–vis) absorption spectra were recorded by using a V-770 (Varian-Cary) spectrophotometer. Bruker D8 Focus diffractometer with Cu-Kα radiation ($\lambda = 0.154$ nm) was used to check the crystal structure of the fabricated samples. X-ray photoelectron spectroscopy (XPS) measurements were performed using a Thermo VG Escalab 250 photoelectron spectrometer.

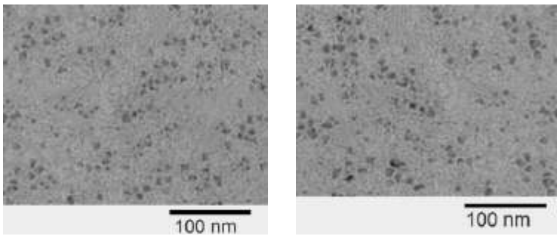

Figure 3. *TEM images of ZnS QDs (on the left) and ZnS:Ce^{3+}/Eu^{3+} QDs (on the right)*

2.2. Structural and compositional analyses of Eu/Ce-doped and (Eu, Ce) co-doped ZnS quantum dots

The surface chemical composition and chemical states of the as-synthesized Ce1% and Eu1% co-doped ZnS QDs were confirmed by X-ray photoelectron spectroscopy (XPS), as illustrated in Fig. 4. The presence of Zn, S, Ce and Eu elements is evidenced by the whole survey spectrum, Fig. 1a. The signal peaks at 881.4 and 899.8 eV were indexed to Ce 3d$_{5/2}$ and Ce 3d$_{3/2}$, respectively (Fig. 1b). In the Eu3d XPS spectra (Fig. 1c), the peaks at 1136.5 and 1166.2 eV are characteristic of Eu 3d$_{5/2}$ and Eu 3d$_{3/2}$, respectively. The splitting energy of 29.7 eV of Eu3d certified the presence of Eu^{3+} ion in ZnS QDs. The presence of Ce3d and Eu3d suggests the successful doping of Ce^{3+} and Eu^{3+} ions in ZnS QDs. The presence of C 1s in the spectrum at 296.8 eV is due to the hydrocarbons in the instrument. The O 1s level observed at 531.6 eV indicates the occurrence of adsorbed oxygen species. No peak corresponding to the impurities is detectable in the spectrum, indicating the high purity of the synthesized sample.

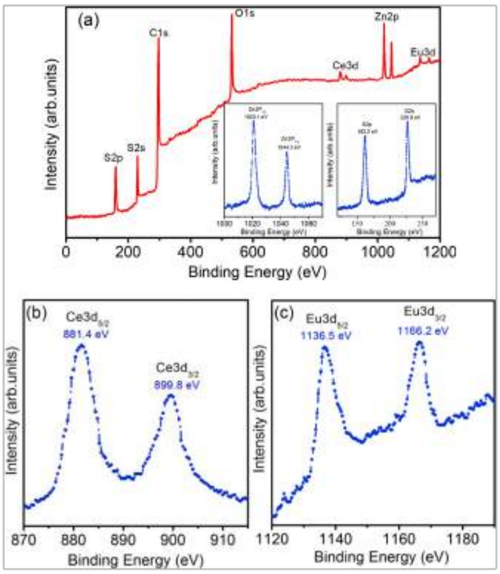

Figure 4. *(a) Survey XPS spectra of the ZnS:Ce1%Eu1% QDs, (b) Ce 3d and (c) Eu 3d.*

The structural characteristics of the synthesized ZnS, ZnS:Eu1%, ZnS:Ce1% and ZnS:Ce1%Eu1-4% QDs were determined by XRD and the results are presented in Figure 5. The diffraction peaks of the undoped ZnS QDs at 2θ ~28.66°, 47.53°, and 56.64° corresponding to the [111], [220] and [311] planes, respectively of the cubic phase of ZnS matching with JCPDF 80-0020. The XRD peaks are broadened due to the nm size of the synthesized samples. The characteristic peaks of the other phases were not observed, indicating the high purity of the product. Compared to the diffraction peaks of the undoped ZnS QDs, those of ZnS:Eu1%, ZnS:Ce1% and ZnS:Ce1%Eu1-4% QDs slightly shifted towards lower angles, indicating an increase in the *d* spacing. The observed shift can be due to the existence of strain because of the incorporation of doping ions into the lattice structure of host ZnS owing to larger radii of Eu^{3+} (107 pm) and Ce^{3+} (97 pm) dopant ions compared to that of Zn^{2+} ion (88 pm). In addition, this shift to lower angles proves that the Ce^{3+} and Eu^{3+} dopant ions substitute the lattice sites of Zn^{2+} ions.

The observed results in Fig. 2 show that the incorporation of dopant does not change the basic crystal structure of ZnS QDs, but it causes the expansion and distortion of the crystal lattice. Thus, the doping is achieved through the substitution of the dopant into the position of the ions in host material. Substitution doping is favorable when the ionic radii of the elements are equivalent and also depend on the dopant concentration.

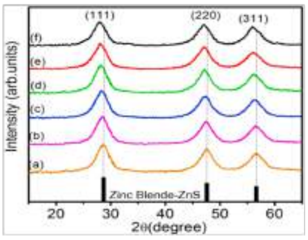

Figure 5. *XRD pattern of (a) ZnS, (b) ZnS:Ce1%, (c) ZnS:Eu1%, (d) ZnS:Ce1%Eu1%, (e) ZnS:Ce1%Eu2% and ZnS:Ce1%Eu4% QDs.*

The crystallite size of the synthesized QDs was calculated by using Debye Scherrer's formula. The calculated parameters from the XRD data i.e. D, a, and d_{hkl} are summarized in Table 1. The calculated values show that the crystallite size of ZnS QDs increases after doping with Eu^{3+} and Ce^{3+} ions.

Table 1
Lattice parameters and crystallite size of the samples.

Sample	2θ	d_{hkl} (nm)	Lattice parameter (nm)	Crystallite size (nm)
ZnS	28.66°	3.12	a = 5.4	2.97
ZnS:Ce 1%	27.52°	3.12	a = 5.41	3
ZnS:Eu1%	28.47°	3.13	a = 5.42	3.06
ZnS:Ce1% Eu1%	28.27°	3.14	a = 5.44	3.15
ZnS:Ce1% Eu2%	28.08°	3.15	a = 5.46	3.24
ZnS:Ce1% Eu4%	27.97°	3.16	a = 5.47	3.29

2.3. Optical properties of Eu^{3+}-doped ZnS quantum dots

In order to obtain the excitation spectrum of ZnS:Eu1% QDs (see in Figủe 6), the excitation wavelength was scanned in the range from 250 nm to 570 nm, whereas the emission wavelength was fixed at 617 nm. There are five narrow peaks in the excitation spectrum of Eu^{3+} ion at wavelengths of 363, 391, 465, 527 and 536 nm. These peaks correspond to the $^7F_0\rightarrow{}^5D_4$, $^7F_0\rightarrow{}^5L_6$, $^7F_0\rightarrow{}^5D_2$, $^7F_0\rightarrow{}^5D_1$ and $^7F_1\rightarrow{}^5D_1$ transitions in $4f^6$ configuration of Eu^{3+} ion, respectively. It can be seen that the $^7F_0\rightarrow{}^5L_6$ (391 nm) and $^7F_0\rightarrow{}^5D_2$ (465 nm) transitions have stronger intensities than the others, so the wavelengths of these peaks are usually used to excite the luminescence of Eu^{3+} ion.

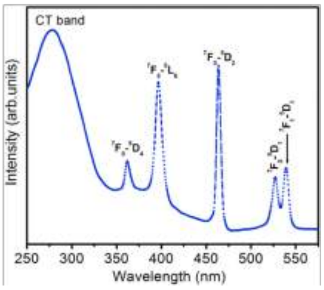

Figure 6. *Excitation spectrum of ZnS:Eu1% QDs.*

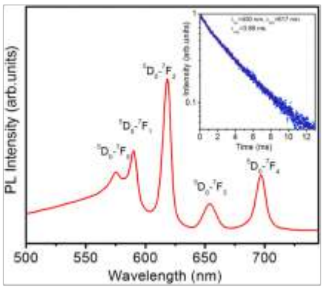

Figure 7. *The PL of ZnS:Eu1% QDs, the inset: PL decay curve of ZnS:Eu1% QDs was measured at wavelength of 617 nm ($^5D_0\rightarrow{}^7F_2$ transition).*

Figure 7 presents the emission spectrum of for ZnS:Eu1% QDs under excitation at 465 nm. The emission spectra consists of five emission peaks of Eu^{3+} ion at 576, 592, 617, 653, and 699 nm correspond to the transitions from the $^5D_0$ level to the $^7F_0$, $^7F_1$, $^7F_2$, $^7F_3$, and $^7F_4$, respectively. For free Eu^{3+} ions, the $^5D_0\rightarrow{}^7F_0$ and $^7F_3$ transitions are strictly forbidden by the Laporte rule. However, these transitions are clearly observed in figure 6a in which the $^5D_0\rightarrow{}^7F_2$ transition at 617 nm wavelength has the strongest intensity. The appearance of these transitions are due to the wave functions mixing between the $^7F_0$, $^7F_3$ and $^7F_2$ levels due to the effect of crystal field perturbation.

In the emission spectra of the Eu^{3+} ion, the $^5D_0\rightarrow{}^7F_2$ transition (red) is called the “hypersensitive transition” and its intensity is strongly influenced by the local environment, whereas the $^5D_0\rightarrow{}^7F_1$ transition is the allowed magnetic dipole, so its intensity is less dependent on the ligand. Therefore, the ratio $R = I(^5D_0\rightarrow{}^7F_2)/I(^5D_0\rightarrow{}^7F_1)$ is often used to estimate the fluorescence efficiency of the red band in some material as well as the ligand asymmetry.

The PL decay curve of the $^5D_0$ state of the ZnS:Eu1% QDs is shown in the inset of figure 7 This curve was measured at wavelength of 617 nm ($^5D_0\rightarrow{}^7F_2$ transition) under excitation at 450 nm. The experiment lifetime (τ_{exp}) of $^5D_0$ state in ZnS:Eu1% QDs was found to be 3.86 ms.

2.4. Influence of Eu and Ce doping on the band gap energy of ZnS QDs

The optical studies of ZnS, ZnS:Eu, and ZnS:Eu, Ce QDs were carried out by UV–visible absorption spectra shown in Figure 8. The UV–vis spectra showed the effect of Eu and Ce substitution on the light absorption and band gap energy (E_g) of ZnS QDs.

Undoped ZnS QDs had a clear UV absorption peak at a wavelength about 292 nm (4.24 eV), which is called the first exciton absorption peak, it can be explained by the transmission of electrons from the valence band to the conduction band of ZnS. This absorption peak shifted strongly towards the shorter wavelengths compared to the ZnS bulk semiconductor (3.66 eV) due to the quantum confinement effect. For Eu, Ce-doped ZnS and (Eu, Ce)-codoped ZnS QDs, the first exciton absorption peaks shifted slightly towards a longer wavelength compared to that of undoped ZnS, demonstrating a decrease in their band gap energy. The decrease in the band gap energy of ZnS:Ce^{3+}, ZnS:Eu^{3+} and (Ce^{3+}, Eu^{3+}) co-doped ZnS QDs compared to undoped ZnS can be due to the increase in particle sizes from XRD, see in Table 1. Besides, these slight shifts may be due to the presence of disorder and defect states due to the Ce^{3+} and Eu^{3+} doping. Eu^{3+} and Ce^{3+} doping creates new electron states near the conduction band of ZnS. Consequently, a new defect band is formed below the conductors, resulting in a band gap reduction. A similar result was also observed for Ce^{3+}, Eu^{3+} co-doped ZnO powder. For the values of the band gap energy, the mean crystal size of the QDs can be determined by using the effective mass approximation formula developed by Brus and Kaynuama. The sizes of the synthesized QDs were determined by effective mass approximation formula and are shown in Table 2.

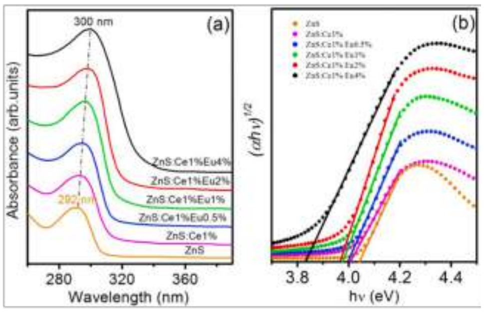

Figure 8. *(a) UV–Vis spectra and (b) the variation of (αhv)2 versus (hv) of the samples.*

Table 2
Particle size and band gap energy of ZnS, ZnS:Eu1%, ZnS:Ce1% and ZnS:Ce1%
Eu1-4% QDs.

Sample	Absorption peak (nm)	Band gap energy (nm)	Particle size (nm)
ZnS	292	4.04	3.2
ZnS:Ce 1%	293	4	3.27
ZnS:Eu1%	295	3.99	3.29
ZnS:Ce1% Eu1%	297	3.98	3.31
ZnS:Ce1% Eu2%	298	3.96	3.34
ZnS:Ce1% Eu4%	300	3.84	3.48

2.5. Energy transfer from Ce^{3+} to Eu^{3+} in ZnS QDs

Curve a in Figure 9 shows the PL spectrum of the ZnS QDs under excitation wavelength at 225 nm. It shows a peak at approximately 320 nm, which is known as excitonic emission due to the recombination of the electrons in the conduction band and the holes in the valence band, and a broad peak with a very low intensity (peak at approximately 475 nm) is assigned to the emission of surface state of the QDs. Curve b in figure 8 presents the PL spectrum of ZnS:Ce^{3+}1% QDs. The PL spectrum exhibits two emission peaks: one peak with low intensity (peak at 324 nm) is known as host emission and the other with greater intensity (peak at 430 nm) is the emission peak of Ce^{3+} ions. Curve c in Figure 9 shows the PL excitation (PLE) spectrum of ZnS:Eu1% QDs monitored at 617 nm. Observed results on Figure 8 show that the emission region of Ce^{3+} ion cover all the excitation peaks of Eu^{3+} ion. This result is very important, it shows the high possibility of the energy transfer from Ce^{3+} ion to Eu^{3+} ion in ZnS QDs co-doped Ce and Eu.

The photoluminescence decay curves of the $5d_1$ level of Ce^{3+} ion in the Ce^{3+} and Eu^{3+} co-doped ZnS QDs were measured with excitation wavelength at 325 nm and monitored at 430 nm ($5d_1 \rightarrow {}^2F_{5/2}$:$Ce^{3+}$ transition), as represented in Figure 10. The obtained decay curves for the emission are non-exponential processes because the photoluminescence is contributed by different origins. The obtained data of the samples are fitted with a tri-exponential function. The average lifetime is calculated and summarized in Table 3. The average decay time were calculated to be 66.22, 45.69, 34.78 ns and 32.03 ns for the Eu^{3+} concentrations of 0, 1, 2 and 4 mol%, respectively. The faster decline of the average decay lifetimes of Ce^{3+} ion with the increasing of Eu^{3+} concentration could be justifiably explained by the introduction of extra decay pathways, which proves the energy transfer process from Ce^{3+} to Eu^{3+} convincingly.

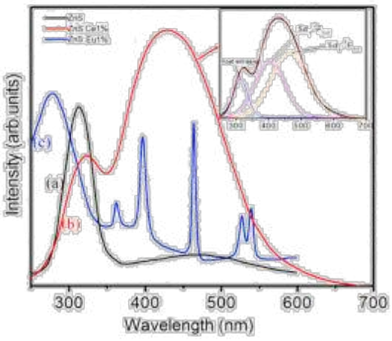

Figure 9. *PL spectra of ZnS, (b) PL spectra of ZnS:Ce1%, and (c) PLE spectra of ZnS:Eu1% QDs.*

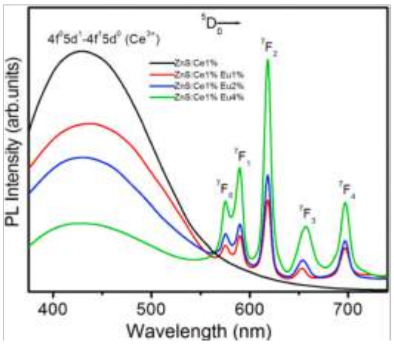

Figure 10. *PL spectra of ZnS:Ce1%Eu(0–4%) QDs.*

From the measured values of the lifetimes, the ET efficiencies from the Ce^{3+} ion to the Eu^{3+} ion are calculated to be 31, 47.47 and 51.63% for the concentrations of 1, 2 and 4 mol% Eu^{3+} ions, respectively. It is noted that the efficiency of ET process significantly increases with the increasing of Eu^{3+} ions concentration. In fact, the increase of the Eu^{3+} concentration reduces the average distance between Ce^{3+} and Eu^{3+} ions. This increases the interaction between Ce^{3+} and Eu^{3+} ions, which leads to the efficiency increase of ET process.

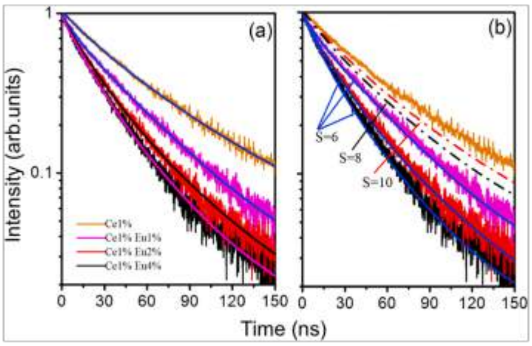

Figure 11. *PL decay curves of ZnS:Ce1% and ZnS:Ce1%Eu1-4% QDs were monitored at 405 nm ($5d_1 \rightarrow {}^2F_{5/2}$:$Ce^{3+}$ transition) under excitation at 325 nm. (a) The solid lines are fitting curves to a tri-exponential function. (b) The solid lines are fitting curves with equation*

$$I(t) = I_0 \exp\left\{ -\frac{t}{\tau_0} - Q\left(\frac{t}{\tau_0}\right)^{3/S} \right\}$$

Table 3

Experimental values of time constants obtained for QDs. The numbers in brackets are the amplitude percentage of each component.

Sample	τ1 (ns)	τ2 (ns)	τ3 (ns)	⟨τ⟩ (ns)
ZnS:Ce1%	24.2 (21.1%)	32.07 (37.6%)	84.23 (41.3%)	66.22
ZnS:Ce1%Eu1%	15.3 (20.7%)	25.72 (34.2%)	56.39 (45.1%)	45.69
ZnS:Ce1%Eu2%	8.3 (19.8%)	18.52 (29.3%)	41.08 (50.9%)	34.78
ZnS:Ce1%Eu4%	7.23 (20.2%)	15.92 (25.6%)	37.1 (54.2%)	32.03

In the ZnS QDs co-doped with Ce^{3+} and Eu^{3+} ions, the ET process from Ce^{3+} to Eu^{3+} can be explained by the direct ET mechanism, which is showed in Figure 12. After being excited by the wavelength of 325 nm, the Ce^{3+} ions jump to the $5d_1$ state. For the Ce^{3+} and Eu^{3+} co-doped ZnS QDs, the $5d_1$ energy state of Ce^{3+} (~28,350 cm^{-1}) is a little higher than the $^5D_4$ energy state of ion Eu^{3+} ion (~27,730 cm^{-1}). Therefor, only one part of the stimulating energy relaxes to the $^2F_{7/2}$ and $^2F_{5/2}$ states of Ce^{3+} ground state creating a broad emission spectra of Ce^{3+} ion and remaining energy part is transferred to the $^5D_4$ state of Eu^{3+}. From $^5D_4$ state, the Eu^{3+} ions quickly recover to the $^5D_0$ state by the multiphonon relaxation. The characteristic emission peaks of Eu^{3+} ion in Figure 10 are due to the radiation recombination of the Eu^{3+} ions from $^5D_0$ state to the ^7F_j (J = 0–4) states.

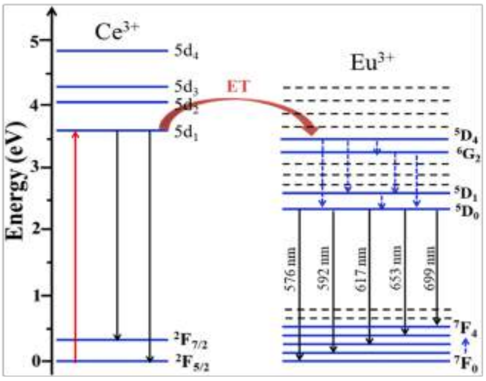

Figure 12. *Energy level diagram and energy processes for* Ce^{3+} *and* Eu^{3+} *co-doped in ZnS QDs under excitation at 325 nm.*

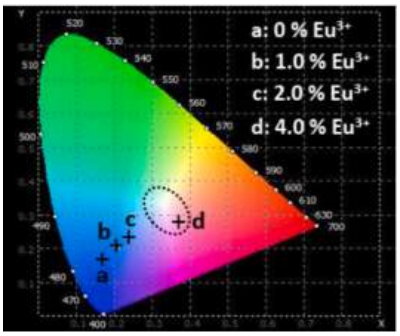

Figure 13 *CIE chromaticity diagram for* $ZnS:Ce^{3+}1\%Eu^{3+}(x = 1–4\%)$ *QDs*.

The emission feature of a material is often estimated through the CIE chromaticity coordinates. In this work, the CIE chromaticity coordinates were calculated by using the PL spectra under an excitation wavelength of 325 nm. The obtained results are shown in Figure 13. It can be seen that the CIE coordinates of $ZnS:Ce^{3+}1\%Eu^{3+}(x = 1–4\%)$ QDs vary systematically from blue (0.167, 0.167) to red orange (0.366, 0.290) with the changes of Eu^{3+} ions' concentration and reached nearly the white area as x = 4%. This is due to the synthesis of two characteristic emission of Ce^{3+} and Eu^{3+} ions. For human visual perception, the value of CCT = 3650K recorded for the sample with $x = 4\%$ corresponds to warm white light. This feature suggests that the Ce^{3+} and Eu^{3+} co-doped ZnS QDs are potential materials for fabricating white light-emitting devices.

2.6. Conclusion

Eu^{3+} and Ce^{3+} co-doped into semiconductor ZnS QDs were synthesized by the chemical method. By using the J-O model, the properties of ligand field and the radiative parameters were calculated for the $^5D_0 \rightarrow {}^7F_2$ transition of ZnS:Eu1% QDs. The small value of Ω_2 indicates that the covalent degree of the Eu^{3+}-ligand bond and the ligand symmetry in semiconductor $ZnS:Eu^{3+}$ QDs are higher than those of the glass host. The obtained results from UV–Vis spectrum showed that the band gap energy of ZnS:Ce, ZnS:Eu and Ce, Eu co-doped ZnS QDs decrease compared to that of undoped ZnS QDs. For Ce^{3+} and Eu^{3+} ions co-doped in ZnS QDs, the luminescence intensity and lifetime of the 5d$_1$ (Ce^{3+}) level decrease while the emission intensity of Eu^{3+} ion increases with the increasing Eu^{3+}concentration. The luminescence quenching and the reduced lifetime of the 5d$_1$ (Ce^{3+}) level are due to the direct ET from Ce^{3+} to Eu^{3+} ion. The ET efficiencies from the Ce^{3+} ions to the Eu^{3+} ions are 31, 47.47 and 51.63% for the concentrations of 1.0, 2.0 and 4.0 mol% Eu^{3+} ions, respectively. The obtained result showed the dipole-dipole interaction plays a major role in the energy transfer process from Ce^{3+} ions to Eu^{3+} ions with a critical distance of 8.26 Å. The CIE chromaticity coordinates showed that the color tone of Eu^{3+} and Ce^{3+} co-doped ZnS QDs was near white at 4.0% Eu^{3+} concentration. This feature suggests that the Ce^{3+} and Eu^{3+} co-doped ZnS QDs are potential materials for fabricating white light-emitting devices.

Chapter 3

SYNTHESIS AND OPTICAL PROPERTIES OF QUANTUM DOTS BASED ON CdSe, CdS DISPERSED IN WATER

This chapter aims to fabricate CdSe/CdS and CdS/ZnS quantum dot systems directly in an aqueous environment, using citrate as a size control agent. These quantum dots have been synthesized under different conditions, especially in the survey, according to the ratio of the citrate trapping agent. With ourresearch group's experience, the size of the quantum dots fabricated by this method has been systematically controlled according to the ratio of the trapping agent. It gives fluorescence emission with the desired colour. A new point of the thesis is that we have fabricated "soluble" quantum dots in water at a low temperature - at 4 ºC.

3.1. Synthesis of CdSe/CdS and CdS/ZnS quantum dots in aqueous solutions

The CdSe/CdS and CdS/ZnS QDs were synthesized using redistilled water and following chemicals: selenium powder (Se), sodium borohydride ($NaBH_4$, 99%), absolute ethanol, $Na_2S\bullet9H_2O$ (98%), $CdCl_2.2.5H_2O$ (99%), trisodium citrate dihydrate (99%), tris (hydroxymethyl) aminomethane (Tris) (99%), hydrochloric acid, sulfuric acid, sodium hydroxide (96%) and $ZnCl_2$. The absolute ethanol Se powder reacted with sodium borohydride to form NaHSe solution; trisodium citrate dihydrate was added into tris-HCl buffer solution with a initial pH value, then cadmium chloride solution were added, forming the solution containing ions Cd^{2+} protected by citrate molecules. The molar ratio (w) of the citrate and the distilled water added for preparing tris-HCl was changed, to receive CdSe QDs with different sizes. After that, H_2Se gas was created by the reaction of above NaHSe solution with diluted H_2SO_4. The H_2Se gas reacted with the above ion Cd^{2+} solution forming CdSe quantum dots. CdSe/CdS QDs solutions were synthesized due to blowing H_2S gas generated by the reaction of Na_2S solution with diluted H_2SO_4 into the CdSe core solutions synthesized as described above with a slow nitrogen flow. The CdS/ZnS QDs were synthesized by the same procedure of synthesizing CdSe/CdS quantum dots. But $ZnCl_2$ was used instead of $CdCl_2$. The size of the QDs was estimated by optical absorption spectra (UV-VIS). The emission characteristics were studed by photoluminescence (PL) spectra.

3.2. Results of synthesis and study of optical properties of CdSe/CdS quantum dots

3.2.1. Visual characteristics, size, shape, and structure of the quantum dots

CdSe/CdS quantum dots were synthesized with the initial molar ratio of Cd:Se:citrate varied to 4:1:10, 4:1:20, and 4:1:30. The obtained samples were transparent and homogeneous solutions, light brown in colour and emitted fluorescent light, with the colour varying depending on the size of the CdSe particles. Figure 14 shows the images of the CdSe/CdS quantum dot solution samples taken under normal light and UV light. The UV light image of white cotton fibers dyed with CdSe/CdS quantum dots is presented in Figure 15. Figure 16 shows the transmission electron microscopy (TEM) images of the synthesized CdSe/CdS quantum dots. The TEM images show that the CdSe/CdS quantum dots existed in the form of clusters and were evenly dispersed in the solution. The size of these quantum dots was estimated to be several nm.

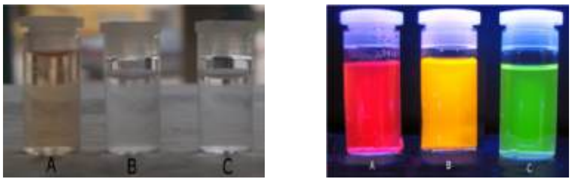

Figure 14. *Photo image of CdSe/CdS QDs samples under normal light (on the left) and UV light (on the right with emission colours as red, yellow and green corresponding to the initial molar ratio of Cd:Se:citrate as 4:1:10; 4:1:20, and 4:1:30, respectively)*

Figure 15. *Ultraviolet light image of white cotton fibers dyed with CdSe/CdS quantum dots.*

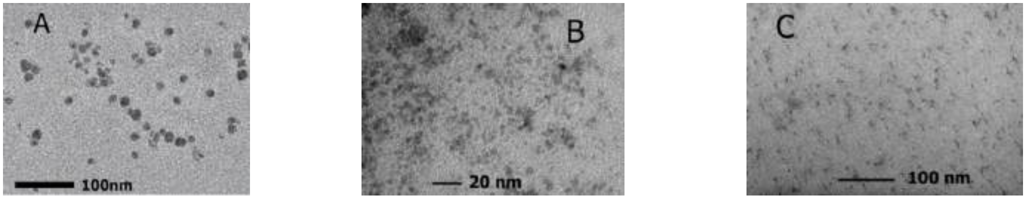

Figure 16. *TEM images of CdSe/CdS QDs with different molar ratios of Cd:Se:citrate: A. 4:1:10; B. 4:1:20; and C. 4:1:30*

The chemical structure of CdSe/CdS quantum dots was determined by Raman scattering. Figure 17 shows the Raman scattering spectrum of CdSe/CdS quantum dots fabricated with a molar ratio of Cd:Se:citrate of 4:1:20 measured on a LABRAM micro-Raman instrument excited by an Argon laser at 488 nm at room temperature. The spectrum has two peaks at wave numbers 206 cm-1 and 297 cm-1, respectively, corresponding to the vibrations of CdSe and CdS crystals. Observing these spectral lines, we can confirm the chemical structure of the quantum dots consisting of two layers, the CdSe core and the CdS shell. The structure of these core/shell nanoparticles has also been confirmed through studies by the research group on the photoluminescence emission spectra of the nanoparticles. It can be seen that the Raman intensity obtained for the CdSe spectral line is much smaller than the Raman intensity of the CdS spectral line. It can be explained by the fact that the CdSe material is located in the nanoparticle's core, so the CdSe's Raman signal obtained is smaller than that of CdS.

Figure 18 shows the X-ray diffraction patterns of CdSe/CdS quantum dot samples fabricated with different molar ratios of the initial materials. The instrument's data shows that there are diffraction lines corresponding to the two materials CdSe and CdS formed in the CdSe/CdS quantum dot material system, in which the CdSe material crystallizes in the directions 002, 102, 103, and the CdS material crystallizes in the directions 110, 112.

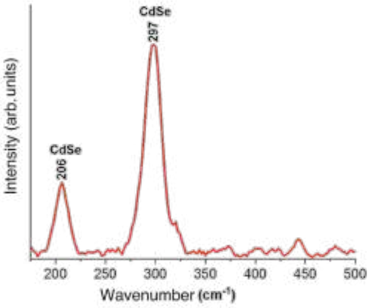

Figure 17. *Raman scattering spectra of CdSe/CdS quantum dots*

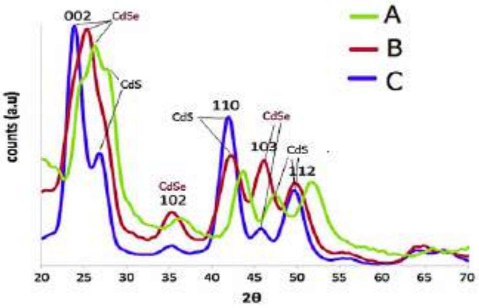

Figure 18. *XRD pattern of CdSe/CdS QDs with the initial molar ratio of Cd:Se:citrate as A. 4:1:10 (w=1); B. 4:1:20 (w=2); và C. 4:1:30 (w=3)*

Experimental results show that the absorption spectra of CdSe and CdSe/CdS quantum dots under the same fabrication conditions for the same CdSe core size do not have much difference in the absorption edge shift. The absorption edges of CdSe and CdSe/CdS quantum dots were determined similarly to those of ZnS and doped ZnS quantum dots in Chapter 2. The absorption edges of CdSe quantum dots changed less after being coated with CdS shells than those of the original CdSe quantum dots. From this, we can deduce the band gap of CdSe core quantum dots for size estimation of CdSe particles. The size of the core CdSe quantum dots is determined through the absorption spectrum according to the Kayanuama formula and is presented in Table 4 according to the w ratio.

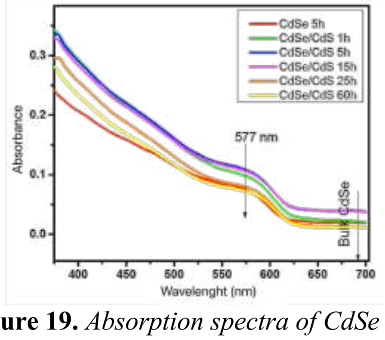

Figure 19. *Absorption spectra of CdSe and CdSe/CdS QDs with the same CdSe core prepared with w = 1*

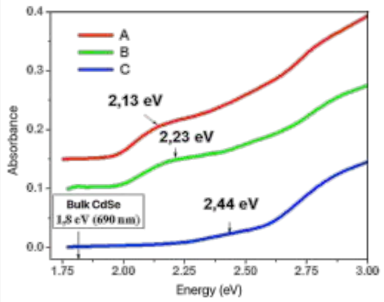

Figure 20. *Absorption spectra of CdSe/CdS QDs with different molar ratios of Cd:Se:citrate. A. 4:1:10; B. 4:1:20; và C. 4:1:30*

Table 4

Size evaluation of CdSe nanoparticles with different trapping agent ratios

Sample	w	Cd:Se:citrate molar ratio	Shift of QDs' absorption edge relative to band gap of bulk CdSe semiconductor (eV)	CdSe QDs' radius (nm)
A	1	4:1:10	0.33	3.8
B	2	4:1:20	0.43	3.6
C	3	4:1:30	0.64	2.7

3.2.2. Flourescent properties of CdSe and CdSe/CdS quantum dots

Figure 21 shows the photoluminescence emission spectra of CdSe and CdSe/CdS quantum dot samples with a w=2 ratio, performed at 4°C and different growth times. The results show that the fluorescence peak shifts towards the long wavelength as the growth time increases. For the sample fabricated at a high temperature of 90ºC (Figure 22), the photoluminescence emission spectra of CdSe samples with CdS shells almost do not shift the peak when changing the growth time. The CdS shell layer plays a vital role in minimizing surface emission and enhancing the fluorescence performance of quantum dots. Controlling the thickness of the shell layer during the fabrication of core/shell quantum dots is important. In our view, to achieve stable emission, quantum dot fabrication needs to be carried out at sufficiently high temperatures.

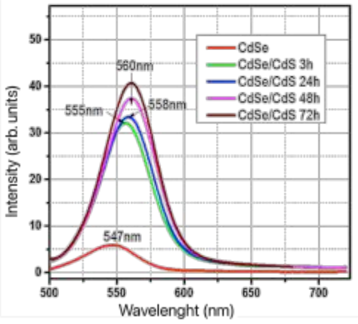

Figure 21. P*hotoluminescence emission spectra of CdSe and CdSe/CdS quantum dot samples with a w=2 ratio, performed at 4 °C and different growth times*

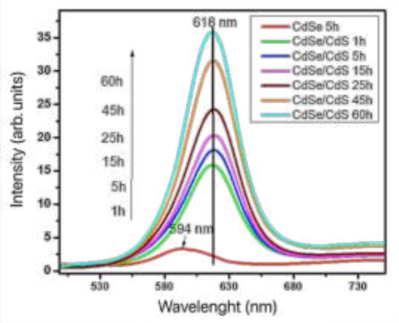

Figure 22. P*hotoluminescence emission spectra of CdSe and CdSe/CdS quantum dot samples with a w=2 ratio, performed at 90 °C and different growth times.*

Figure 23 presents the photoluminescence emission spectra of CdSe quantum dots fabricated with varying molar ratios of citrate at 45°C, recorded under 480 nm excitation light at room temperature. The emission peaks were observed at 614 nm, 587 nm, and 568 nm, corresponding to Cd:Se:citrate molar ratios of 4:1:10; 4:1:20, and 4:1:30, respectively. The results show that the fluorescence intensity is highest for the sample with citrate concentration corresponding to w = 2. However, emission bands at the long wavelength are also observed in the fluorescence spectrum. These emissions are attributed to surface emissions and may be caused by charge imbalances on the surface of the nanoparticles when the amount of citrate is large. Figure 24 shows that the emission of the surface states in the long wavelength range of CdSe/CdS quantum dots is significantly reduced compared to that of uncoated CdS-coated CdSe nanoparticles, and the intrinsic emission is enhanced. Table 5 gives information on the widths of the fluorescence spectra of CdSe/CdS quantum dots as a function of w corresponding to their emission colours.

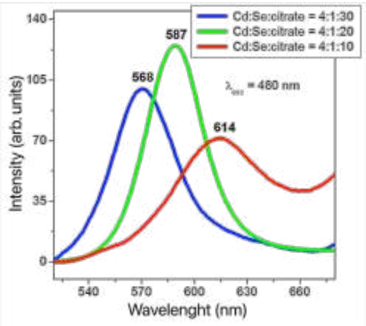

Figure 23. *Photoluminescence spectra of CdSe QDs samples with different w ratios under the excitation of 480 nm at room temperature*

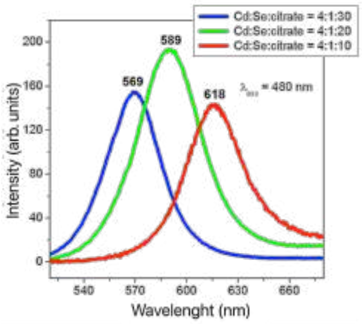

Figure 24. *Photoluminescence spectra of CdSe/CdS QDs samples with different w ratios under the excitation of 480 nm at room temperature*

Table 5
Photoluminescence emission spectral width of CdSe/CdS quantum dots with different trapping ratios corresponding to different emission colors

Sample	w	Cd:Se:citrate molar ratio	Emission peak (nm)	Full width at half maximum (FWHM) (nm)	Emission colour
A	1	4:1:10	619	41	Orange-red
B	2	4:1:20	589	43	Yellow
C	3	4:1:30	569	37	Green

The CdSe and CdSe/CdS quantum dot samples show changes in their optical properties with storage time regarding the fluorescence emission peak and the emission intensity (Figures 25 and 26). The blue shift of the fluorescence spectra of the quantum dots after a storage period can be explained by the change in the surface charge state and the combined effective electric field applied to the electronic transitions, increasing the energy of these levels. The passivation of the Se^{-2} and Cd^{2+} open bonds can explain the observed increase in fluorescence intensity after a certain storage period. However, it can be seen that if the storage period is too long, the fluorescence of the samples is reduced due to the aggregation of the quantum dots.

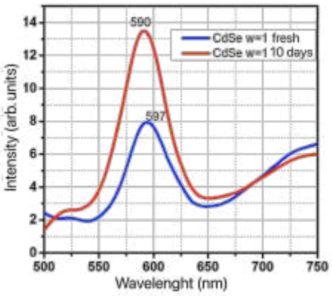

Figure 25. *Photoluminescence spectra of CdSe QDs as grown and after preparation.*

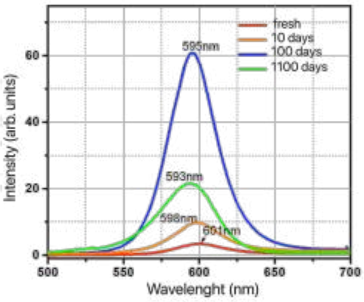

Figure 26. *Photoluminescence spectra of CdSe/CdS QDs as grown and after preparation.*

Figure 27 shows the normalized fluorescence spectra of CdSe core quantum dots prepared with w = 1 and varying growth time. It is easy to see that as the growth time increases, the fluorescence peak shifts toward longer wavelengths, indicating that the particle size increases with time, which is also consistent with the absorption spectra. Therefore, the growth time plays an essential role in influencing the emission properties of quantum dots, especially their emission wavelength. However, to improve the photostability, adding a CdS shell must protect the quantum dots.

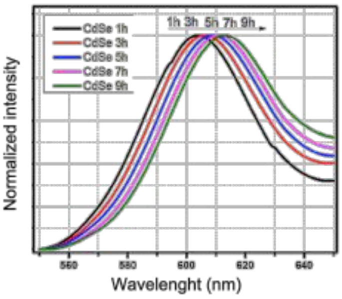

Figure 27. *Normalized photoluminescence spectra of CdSe QDs prepared with w =1 and varying growth time under excitation wavelenght of 470 nm*

Figure 28 shows the fluorescence spectra of CdSe/CdS quantum dots synthesized at 4 ºC compared with those of CdSe/CdS quantum dots synthesized at 75 ºC with the same initial concentrations. The fluorescence peak of the low-temperature sample was observed to be shifted toward the short wavelength compared to the high-temperature sample. The fluorescence spectrum of the low-temperature sample was Gaussian symmetric, and the surface-emission was almost limited. However, the fluorescence intensity of this sample was much lower than that of the high-temperature sample. Thus, the temperature for the synthesis process plays an important role in affecting the size and optical properties of CdSe quantum dots. However, the optimal fabrication temperature selection still needs to be carried out through further studies.

The photoluminescence kinetics of CdSe/CdS quantum dots were also investigated. The results showed that the average photoluminescence lifetimes of the samples were 25.24 ns, 25.97 ns and 27.64 ns for the samples with core growth times of 1 hour, 5 hours and 9 hours, respectively. Samples with longer fluorescence lifetimes generally respond better to experimental applications. Therefore, prolonged quantum dots' prolonged core growth will improve their emission quality.

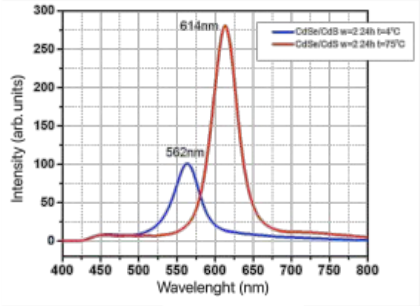

Figure 28. *Photoluminescence spectra of CdSe/CdS quantum dots prepared with w=2 and the synthesis temperatur of 4ºC anđ 75ºC*

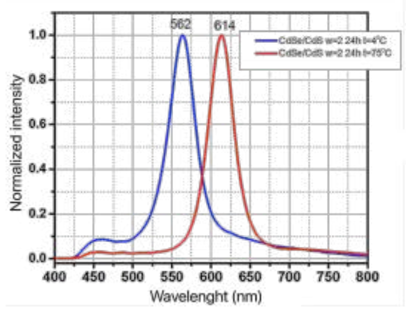

Figure 29. *Photoluminescence spectra of CdSe/CdS quantum dots prepared with w=2 and the synthesis temperatur of 4ºC anđ 75ºC*

Thêm h32

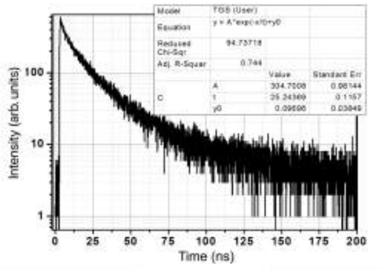

Figure 30. *PL decay curve of CdSe1h/CdS10h QDs*

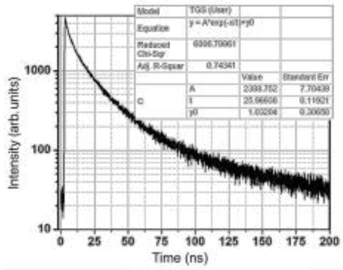

Figure 31. *PL decay curve of CdSe5h/CdS10h QDs*

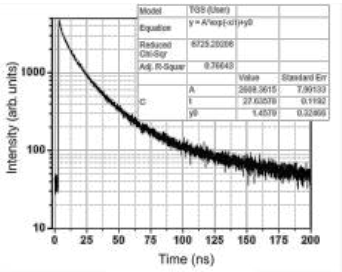

Figure 32. *PL decay curve of CdSe9h/CdS10h QDs*

3.3. Results of synthesis and study of optical properties of CdS/ZnS quantum dots

3.3.1. Visual characteristics, size, shape, and structure of the quantum dots

Figure 33 shows the images of CdS/ZnS quantum dot solutions dispersed in water under ultraviolet light, emitting fluorescence in the blue region. Figure 34 shows the transmission electron microscopy (TEM) images, showing that these nanoparticles are uniformly dispersed in water and have the shape of small dots. This dispersion is ensured by the citrate surfactant adhering around the quantum dots. Based on TEM observations, the size of these particles is estimated to be between 3 and 5 nm.

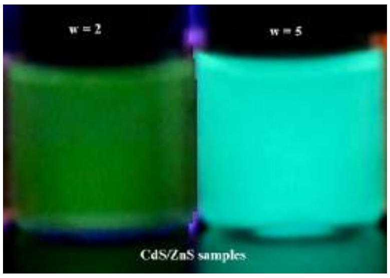

Figure 33. *Photo image of CdS/ZnS QDs samples under UV light*

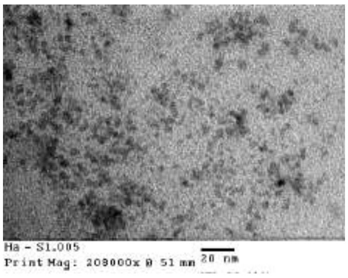

Figure 34. TEM *image of CdS/ZnS QDs w = 5*

The X-ray diffraction results of the CdS/ZnS nanoparticle samples were also investigated. The results showed that the crystallization efficiency of the samples was still inefficient, not reaching the level as good as quantum dots fabricated in solvents at high temperatures. It can be explained by the fact that the CdS/ZnS nanomaterials have not achieved the desired crystallization in aqueous medium, as required by experimental conditions. It is necessary to find more optimal conditions for this process. The diffraction patterns also showed that CdS has a greenockite structure, while ZnS has a hexagonal wurtzite structure. This feature, together with the width of the diffraction lines, suggests that the particles are nanometer in size.

The size of the dots is also estimated from their absorption spectra. From the two absorption spectra in Figures 35 and 36, we can also determine the absorption edge positions of the CdS/ZnS quantum dots similarly to the determination of the absorption edge of the ZnS quantum dots in

Chapter 2. Specifically, these positions are ~447 nm (for w = 2) and ~435 nm (for w = 5). Notably, these absorption edge values are shifted significantly toward the blue wavelength compared to the absorption edge of the bulk CdS semiconductor ($\lambda_{\text{Cds khối}}$~500 nm). This shift toward the blue wavelength of the absorption edges suggests that the CdS nanoparticles are in the strong quantum confinement regime.

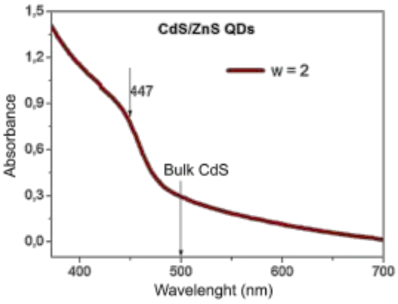

Figure 35. *Absorption spectra of CdS/ZnS prepared with w = 2*

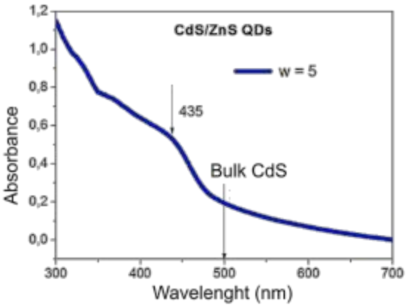

Figure 36. *Absorption spectra of CdS/ZnS prepared with w = 5*

3.3.2. Flourescent properties of CdS and CdS/ZnS quantum dots

Figures 37 and 38 show the photoluminescence emission spectra of CdS and CdS/ZnS quantum dots synthesized at w = 2 under the same conditions. Both spectra have emission peaks at ~470 nm and ~485 nm. These peaks are refered to the emission of CdS nanoparticles, and shifted towards the short wavelength quite a bit compared to the absorption edge of bulk CdS semiconductor. However, the CdS particle size in the sample is not uniform and surface emission is still observed. The results obtained are similar to those for the w = 5 sample. It suggests that the ZnS capping of CdS nanoparticles has not yet been perfected by the direct fabrication of this type of quantum dot in aqueous medium because ZnS is difficult to form at low temperature. This is also a challenge and requires further detailed investigation.

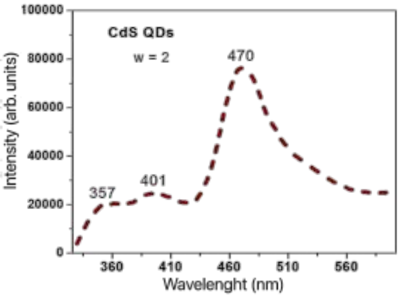

Figure 37. *Photoluminescence spectra of CdS QDs prepared with w=2*

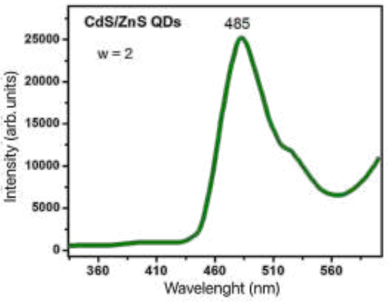

Figure 38. *Photoluminescence spectra of CdS/ZnS QDs prepared with w=2*

Chapter 4

SYNTHESIS AND OPTICAL PROPERTIES OF SILICA NANOPARTICLES CONTAINING QUANTUM ĐOTS

4.1. Synthesis of silica nanoparticles containing quantum đots via Stöber method

We fabricated silica nanoparticles containing quantum dots using the Stöber method without surfactants. The method is known as a convenient method, using non-toxic chemicals. It can directly coat quantum dots with silica shells to form luminescent silica nanoparticles with luminescent centers being quantum dots dispersed in water or alcohol, easily dispersing them into buffer solutions for different uses.

The quantum dots that the thesis has fabricated are the quantum dots used to coat the silica shell. These quantum dot systems all belong to the $A^{II}B^{VI}$ group, including CdSe/CdS and CdS/ZnS in a citrate environment, so they all have carboxyl COO- functional groups on the surface, creating negative charges. Since the silica matrix synthesized by sol-gel method also has negative charge, to ensure that the quantum dots can be effectively encapsulated into the silica matrix, it is necessary to neutralize their surface charge. Aminopropyl triethoxsilane (APTES) was chosen as a surface charge neutralizer of the quantum dots before they were incorporated into the silica matrix because APTES does not affect the optical properties of the quantum dots and does not affect the hydrolysis and condensation processes during the synthesis of silica nanoparticles.The experimental procedure for fabricating silica nanoparticles containing quantum dots was carried out according to the diagram in Figure 39. The samples after being fabricated were also cleaned by centrifugation in alcohol using a dialysis bag at a speed of 10,000 rpm. After at least 5 washings, the particles were dispersed in different pH environments for research purposes..

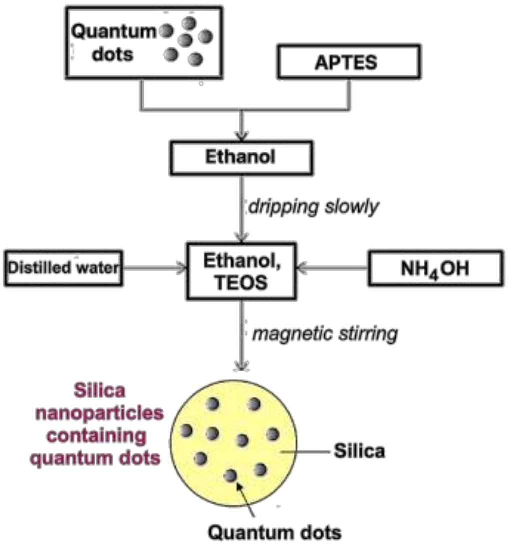

Figure 39. *Flowchart of the synthesis of silica nanoparticles containing quantum dots by Stöber method*

4.2. Results of synthesis and properties of $CdSe/CdS/SiO_2$

4.2.1. Results of synthesis and properties of $CdSe/CdS/SiO_2$

The obtained $CdSer/CdS/SiO_2$ nanoparticle samples were ivory-white solutions, which is the colour of silica, in which CdSe/CdS/SiO2 nanoparticles were dispersed. Figure 40 shows photographs of the solution samples containing $CdSe/CdS/SiO_2$ nanoparticles prepared with different citrate ratios. The TEM image (Figure 41) shows that the silica nanoparticles were formed in a spherical, homogeneous, and monodisperse form in the solution..

Various experiments showed the best fluorescence emission intensity for silica nanoparticles containing CdSe/CdS quantum dots with a Cd:Se:citrate ratio of 4:1:20 (corresponding to w = 2). Therefore, the investigation conditions for silica nanoparticles containing CdSe/CdS quantum dots were carried out on a CdSe/CdS quantum dot sample system synthesized with a w = 2 ratio.

Figure 40. *Image of $CdSer/CdS/SiO_2$ nanoparticles solution samples with w = 1 (A), w = 2 (B), and w= 3 (C)*

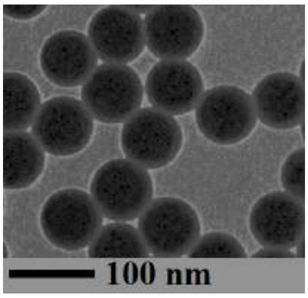

Figure 41. *TEM image of $CdSer/CdS/SiO_2$ nanoparticles*

The size distribution of silica nanoparticles containing CdSe/CdS quantum dots was also investigated by measuring the Dynamic Light Scattering (DLS) and zeta potential. The results showed that the size of the particles was relatively uniform, which was quite similar to the size obtained from TEM images.

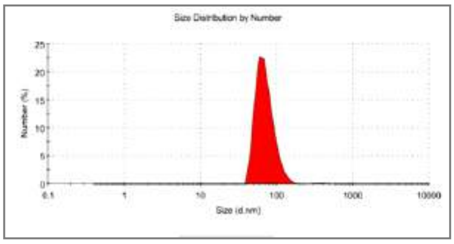

Figure 41. *Size distribution of CdSer/CdS/SiO_2 nanoparticles*

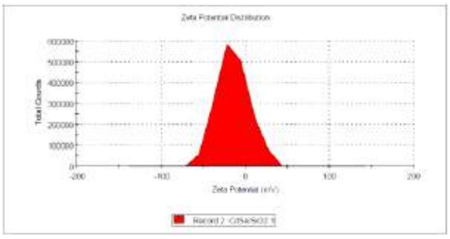

Figure 42. *Zeta potential distribution of CdSer/CdS/SiO_2 nanoparticles*

4.2.2. Effect of NH_4OH catalysis quantity on characterizations of CdSe/CdS/SiO_2 nanoparticles

The results showed that under experimental conditions, when using a catalyst amount of 400µl (on 15 ml of the total solution), the CdSe/CdS/SiO2 nanoparticles formed had the most uniform round shape and size. In the experiments, the variation of the catalyst amount was tested, and the results showed that the nanoparticles had a more uniform round shape when using a more significant catalyst amount, indicating the role of the catalyst in the hydrolysis and condensation reaction.

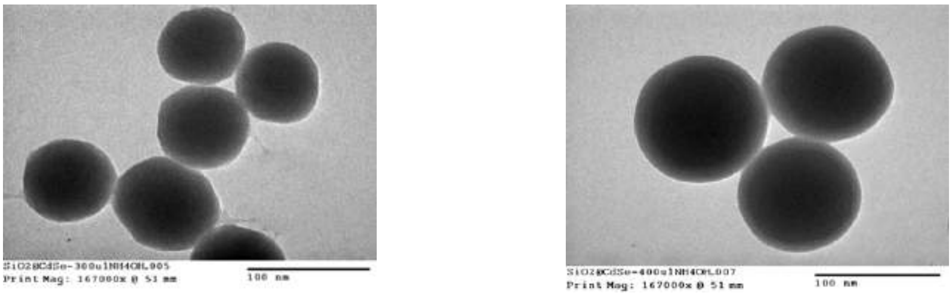

Figure 43. *TEM images of CdSe/CdS/SiO_2 nanoparticles synthesized with 300 µl NH_4OH (on the left) and 400 µl NH_4OH (on the right) (the initial molar ratio was prepared as TEOS:H_2O:APTES = 15000:713:1,5)*

The absorption and fluorescence spectra of CdSe/CdS/SiO2 nanoparticles synthesized with different catalyst amounts are shown in Figures 44 and 45. Absorption spectra analysis shows that the absorption of CdSe/CdS/SiO2 nanoparticle samples is higher than that of CdSe/CdS quantum dots without silica shell due to the contribution of silica matrix to the absorption.

When the catalyst amount is low (200 µl), the fluorescence intensity of CdSe/CdS/SiO2 nanoparticles is significantly lower than that of the silica-uncoated quantum dots that have not yet formed an utterly spherical shape due to the high pH environment that is sufficient to stimulate hydrolysis and condensation, resulting in the quantum dots not being entirely encapsulated by the silica shell, which results in lower fluorescence intensity. When the amount of NH4OH increased to 300 µl, the fluorescence intensity of the quantum dots in the silica matrix increased, indicating that the silica shell better passivated the surface of the quantum dots. At the same time, the appropriate reaction medium produced silica particles containing better dispersed quantum dots, leading to an increase in fluorescence intensity. However, when the amount of catalyst increased to 400 µl, the fluorescence intensity of the CdSe/CdS/SiO2 nanoparticles decreased, lower than that of the CdSe/CdS quantum dots without silica coating. The reason may be that the free quantum dots cannot be covered entirely in the silica matrix, and there may be many holes in the silica matrix, leading to the quantum dots being detached from the matrix when dispersed into the medium and lost during the centrifugation and purification processes.

.

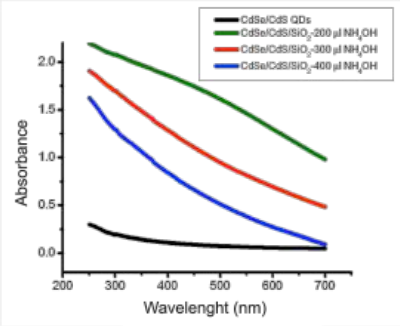

Figure 44. *Absorption spectra of CdSe/CdS/SiO₂ nanoparticles with different catalysis amounts*

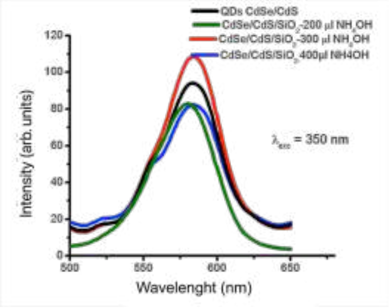

Figure 45. *Photoluminescence spectra of CdSe/CdS/SiO₂ nanoparticles with different catalysis amounts*

4.2.3. Effect of NH_4OH catalysis quantity on characterizations of $CdSe/CdS/SiO_2$ nanoparticles

The amounts of $CdSe/CdS/SiO_2$ nanoparticles with the change of TEOS precursor were 50 µl, 100 -l, and 150 µl. In the experiments synthesizing $CdSe/CdS/SiO_2$ nanoparticles, the amount of TEOS used was 150 µl (over 15 ml of total solution volume), which gave the most round and uniform-sized CdSe/CdS/SiO2 nanoparticles.

The fluorescence intensity was highest when the TEOS amount was 150 µl, although the quantum dot amount added during fabrication was the same for all samples. This phenomenon can be explained by the fact that when the TEOS amount was low, the silica nanoparticles were not formed uniformly, leading to a small amount of quantum dots being incorporated into the silica particles and possibly lost during fabrication and cleaning. Therefore, the fluorescence intensity would be low. When the TEOS amount was increased, the silica nanoparticles formed more evenly and rounded, adding more quantum dots to the silica matrix. This led to an increase in fluorescence intensity due to more quantum dots being encapsulated in the silica matrix.

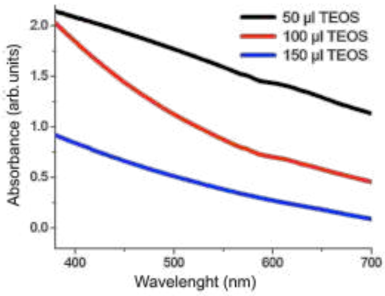

Figure 46. *Absorption spectra of CdSe/CdS/SiO₂ nanoparticles with different TEOS amounts*

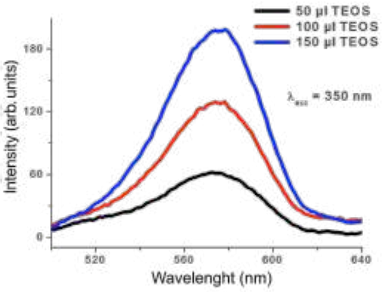

Figure 47. *Photoluminescence spectra of CdSe/CdS/SiO₂ nanoparticles with different TEOS amounts*

4.2.4. Effect of H_2O quantity in reaction for the formation of silica nanoparticles

The results obtained for the optical properties show that the most suitable water amount is ~700 µl. Therefore, in order to obtain good sample quality and the highest luminescence ability, the catalyst conditions and the amount of APTES will be adjusted according to the amount of water. The best fluorescence intensity is achieved using samples prepared with 700-800 µl water. However, if the amount of water continues to increase, the fluorescence intensity of the samples will tend to decrease. Dependence of fluorescence intensity of CdSe/CdS/SiO2 nanoparticles on the amount of water participating in the reaction.

4.2.5. Effect of APTES quantity

The research results of the thesis show that the most optimal amount of APTES can be in the range of 3 to 9 µl. Figure 48 shows the dependence of the fluorescence intensity of CdSe/CdS/SiO2 nanoparticles on the amount of APTES participating in the reaction. The most optimal amount of reactant to produce CdSe/CdS/SiO2 nanoparticles with uniform size, monodisperse and the best fluorescence emission is 300 µl NH4OH, 150 µl TEOS, 1.5 µl APTES, 713 µl H2O.

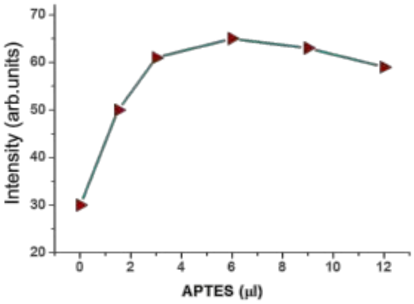

Figure 48. T*he dependence of fluorescence intensity on the amount of APTES participating in the reaction to form CdSe/CdS/SiO*$_2$ *nanoparticles*

4.2.6. Optical quality of nanoparticles over storage time

After about one month of storage, the fluorescence intensity of silica nanoparticles containing quantum dots decreased by ~50% compared to the initial value. After about three months, it became more stable and did not decrease much..

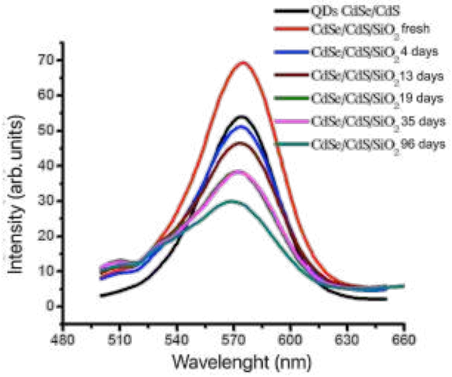

Figure 49. *Photoluminescence spectra over storage time of CdSe/CdS/SiO*$_2$ *samples*

4.3. Results of research and synthesis of CdS/ZnS/SiO2 nanoparticles

4.3.1. Results of synthesis of CdS/ZnS/SiO$_2$ nanoparticles

The fabrication of CdS/ZnS quantum dots in a water/citrate medium at temperatures below 100°C poses a challenge because ZnS semiconductors are difficult to form at low temperatures. However, this method helps to minimize the toxicity during the synthesis of quantum dots. After fabrication, CdS/ZnS quantum dots were dispersed in water and then coated with a silica shell using the Stöber method, similar to the fabrication process of CdSe/CdS/SiO2 nanoparticles. The silica coating, as studied, will help enhance the advantages of these nanoparticles in biomedical applications such as fluorescent markers and biological imaging. The study's results on the fabrication of CdS/ZnS/SiO$_2$ nanoparticles were investigated based on the change in the amount of NH_4OH catalyst.

Figure 50 shows the TEM image of the silica nanoparticle sample containing CdS/ZnS quantum dots according to the amount of catalyst present in the reaction. The rightmost image of Figure 50 is an image of CdS/ZnS/SiO2 nanoparticles synthesized with 450 µL of 15 mL of the total solution, including an HR-TEM image taken from a region in a SiO$_2$ nanoparticle. The crystalline region in the SiO$_2$ particle observed in this image is attributed to the silica nanoparticle's CdS/ZnS quantum dots. The SiO$_2$ nanoparticles are not clearly formed with a small amount of catalyst. However, it is possible to observe that the SiO2 clusters aggregate into particles with an average size of 60-80 nm. When the catalyst dose is increased to 300 µL, the SiO$_2$ nanoparticles have more explicit grain boundaries. When the catalyst dose is increased by 4.5 times, the silica nanoparticles form quite round with relatively smooth surfaces, with 100-120 nm sizes. However, the survey results indicate that with higher catalyst doses, the emission of the quantum dots will be affected, similar to the case of CdSe/CdS quantum dots.

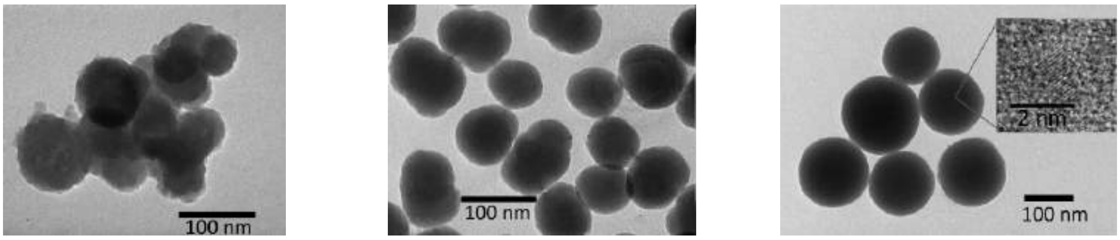

Figure 50. *TEM images of the TEOS:Cd:NH_4OH molar ratios from left to right are 1.5:4:1; 1.5:4:3, and 1.5:4:4.5 of silica nanoparticles containing CdS/ZnS quantum dots*

4.3.2. Optical properties of CdS/ZnS/SiO_2 nanoparticles

Figure 51 shows the optical absorption spectra of CdS/ZnS/SiO2 nanoparticles according to the catalyst dosage and compared with the optical absorption spectra of uncoated CdS/ZnS quantum dots with the same quantum dot concentration. The optical absorption spectra of CdS/ZnS/SiO2 nanoparticles were steep and challenging to define, unlike the absorption edges of uncoated CdS/ZnS quantum dots.

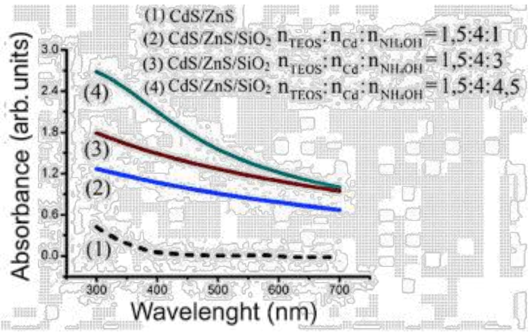

Figure 51. *Absorption spectra of CdS/ZnS/SiO2 nanoparticles with the amount of catalyst (lines 2, 3, 4), and absorption spectra of CdS/ZnS quantum dots without silica (line 1)*

Figure 52 presents the photoluminescence spectra of CdS/ZnS/SiO2 nanoparticles. The fluorescence emission intensity of the sample was reduced for the CdS/ZnS/SiO2 nanoparticle sample synthesized with the most significant amount of catalyst (line 4, Figure 52). However, the resulting silica nanoparticles were more uniform and had a spherical shape and an obvious grain boundary. This reduction can be explained by the large amount of catalyst present in the nucleation reaction, which increased the pH of the solution, leading to a decrease in the emission of CdS/ZnS quantum dots in the silica matrix. Therefore, the careful consideration in choosing an appropriate catalyst ratio, which is sufficient to form silica nanoparticles but does not reduce the fluorescence emission of quantum dots, is crucial for obtaining silica nanoparticles containing quantum dots with the best emission intensity.

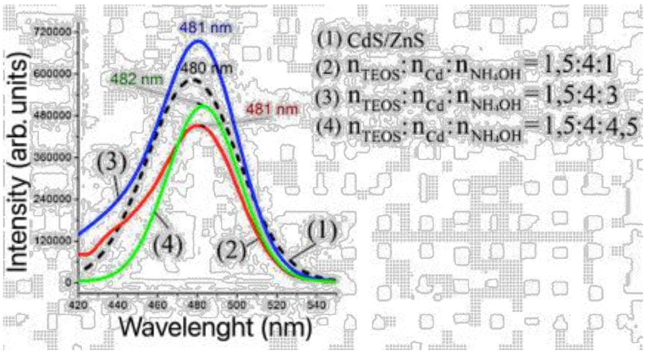

Figure 52. *Fluorescence spectra versus reaction catalyst of CdS/ZnS/SiO2 nanoparticles*

Figure 53 shows the fluorescence decay spectra versus time of CdS/ZnS/SiO_2 nanoparticles and CdS/ZnS quantum dots without silica shell under a laser excitation wavelength of 405 nm and fluorescence emission wavelength of 480 nm. By multi-exponential ensemble analysis, the average lifetime of CdS/ZnS/SiO2 nanoparticles was estimated to be ~ 38.6 ns, longer than the average lifetime of CdS/ZnS nanoparticles without silica shell (~ 33.5 ns). This increase in luminescence lifetime can be explained by the stability of the emission of CdS/ZnS quantum dots in the silica matrix, and the surface of the quantum dots is also protected by the silica shell, leading to a longer lifetime. This has important implications for the application of CdS/ZnS/SiO2 nanoparticles in fluorescent labelling applications.

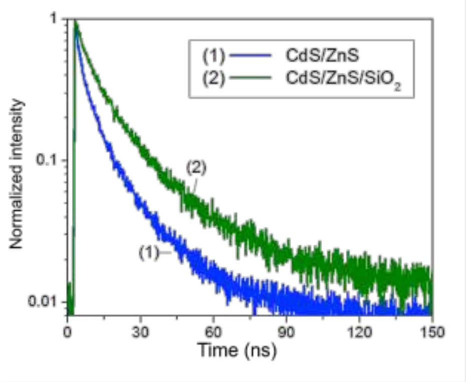

Figure 53. *Fluorescence decay curves of CdS/ZnS/SiO$_2$ nanoparticles and non-silica-coated CdSe/CdS quantum dots under the same conditions.*

CONCLUSION

1. Successfully fabricated ZnS and ZnS quantum dots doped and co-doped with rare earth ions Eu^{3+} and Ce^{3+} in solvents at high temperatures. The radiation parameters were calculated for the transitions of Eu^{3+} and Ce^{3+} ions in the ZnS lattice. The band gap energies of ZnS:Ce, ZnS:Eu and ZnS quantum dots co-doped with Eu^{3+} and Ce3+ ions were reduced compared to those of undoped ZnS quantum dots. The energy transfer mechanism between Ce and Eu ions in ZnS quantum dots was studied and explained for the first time. The energy transfer process from Ce^{3+} ions to Eu^{3+} ions was attributed to dipole-dipole interaction with a critical transfer distance of 8.26 Å. The CIE colour coordinates showed that the colour tone of ZnS quantum dots co-doped with Eu^{3+} and Ce^{3+} was almost white at a Eu^{3+} concentration of 4.0%. This feature promises that ZnS quantum dots co-doped with Ce^{3+} and Eu^{3+} ions are potential materials for fabricating white light-emitting devices.

2. Successfully synthesized CdSe/CdS and CdS/ZnS quantum dots dispersed in water using citrate trapping agent - a safe method with low toxicity chemicals, especially low sample preparation temperature. The fabricated material sample systems are transparent solutions containing quantum dots, emitting strong fluorescence under ultraviolet light; the fluorescence emission colour depends on the size of the core quantum dot. The size of the core quantum dots increases with increasing sample growth time. The optical properties of the quantum dots have been systematically investigated, depending on the concentration of the trapping agent citrate. The quantum dots have good luminescence quality, with a luminescence lifetime of several tens of ns, suitable for use as fluorescent markers.

3. Successfully fabricated silica nanoparticles containing CdSe/CdS and CdS/ZnS quantum dot systems by the Stöber method. The silica nanoparticles are spherical and monodisperse in solution, with sizes ranging from ~70 - 150 nm depending on the synthesis conditions. The nanoparticles' morphology, size, dispersion and optical properties were thoroughly investigated under different fabrication conditions. These silica nanoparticles with luminescent centres as quantum dots have promising applications in many labelling fields. The luminescence lifetime of silica nanoparticles containing quantum dots is longer than that of free quantum dots.

LIST OF THE PUBLICATIONS RELATED TO THE DISSERTATION

1. **Chu Anh Tuan**, Ngo Van Hoang, Trinh Duc Thanh Giang, Nguyen Thi Lan, Dinh Thi Ha, Nguyen Thi Thanh Xoan, Vu Thi Thanh Hương, Le Tien Ha, Nguyen Thi Lan Anh, Chu Viet Ha, Tran Hong Nhung, and Vu Thi Kim Lien "CdSe/CdS nanoparticles in aqueous solution: fabrication and optical characterization", *Proceedings of the National Conference on Solid State Physics and Materials Science* – SPMS, 2017, ISBN: 978-604-95-0325-2.

2. Chu Viet Ha, Ngo Van Hoang, **Chu Anh Tuan**, Phạm Thuy Anh, Nguyen Ngoc Le, Vu Thị Kim Lien. Blue – Green emission of CdS quantum dots dipersed in citrate aqueous solution. *Proceedings of the National Conference on Solid State Physics and Materials Science – SPMS 2017.* ISBN: 978-604-95-0325-2

3. **C.A. Tuan**, V.H. Yen, K.C. Cuong , N.T.M. Thuy, P.M. An, N.TB. Ngoc, D.T. Hue, A. Xayyadeth, Y.Peng, N.N. Le, N.T.K. Van, L.T. Ha, N.T. Kien, C.V.Ha. Optical properties and energy transfer mechanism of Eu^{3+}, Ce^{3+} doped and co-doped ZnS quantum dots. *Journal of Luminescence*, Volume 236, 2021, 118106 (ISI, Q2, IF = 3,28).

4. Chu Viet Ha, **Chu Anh Tuan**, Nguyen Thi Bich Ngoc, Nguyen Quang Liem, Vu Thi Kim Lien. Synthesis and Optical Characterizations of the Fluorescence Silica Nanoparticles Containing Quantum Dots. 2020. *VNU Journal of Science: Mathematics-Physics*, 36 (2)

5. **Chu Anh Tuan**, Vu Thi Kim Lien, Nguyen Thi Hang Nga, Nguyen Ngoc Le, Nguyen Thi Bich Ngoc, Ngo Van Hoang, Chu Viet Ha,. Effect of Electric Neutralizer (APTES) on Optical Properties Of Silica Nanoparticales Containing CdSe/CdS Quantum Dots. *Advances in Optics, Photonics, Spectroscopy & Applications XI*, 2021, pp 153-156, ISBN: 978-604-9988-20-2

6. **Chu Anh Tuan**, Vu Thi Kim Lien, Do Minh Hoat, Vu Thi Hong Hanh, Nguyen Thanh Binh, Le Tien Ha, Chu Viet Ha, Optical Characterization of Ce doped ZnS Quantum Dots. 2023. *Proceedings of The XIII National Conference on Solid State Physics and Materials Science XIII* – SPMS 2023, 432-436.

7. Vu Thi Kim Lien, Do Minh Hoat, **Chu Anh Tuan**, Tran Thi Bich, Doan Quang Huy, Le Tien Ha, Nguyen Thi Bich Ngoc, Ngo Van Hoang, Chu Viet Ha. Effect of precursor and catalysts amounts on optical properties of silica nanoparticales containing CdSe/CdS Quantum dots. 2023. *Proceedings of The XIII National Conference on Solid State Physics and Materials Science XIII* – SPMS 2023, 172-178.

8. **Chu Anh Tuan**, Vu Thi Kim Lien, Vu Van Khai, Dương Thi Phuong Chi, Le Tien Ha, Chu Viet Ha, Optical Characterizations of CdS/ZnS and CdS/ZnS/SiO2 Nanoparticles For Labelling Applications, *TNU Journal of Science and Technology*, 228(10): 287 - 295 2023 (ACI index).

9. **Chu Anh Tuan,** Chu Viet Ha, Patent for Utility Solution: "Process for synthesizing $A^{II}B^{VI}$ core-shell structured semiconductor quantum dot materials in aqueous medium for fluorescent labeling applications", has been accepted as a valid application by the National Office of Intellectual Property, Ministry of Science and Technology of Vietnam, No. 103540/QD-SHTT Decision on acceptance of valid application by the National Office of Intellectual Property, September 28, 2024